Microwave Engineering
Ulm University

universität ulm

Evaluating Error Influences of a Dielectric Waveguide for mm-Wave In Vitro Epithelial Cell Vitality Measurements

Philipp Hinz, Mario Mueh, Jessica Heck, Christian Damm

DOI: na

Evaluating Error Influences of a Dielectric Waveguide for mm-Wave In Vitro Epithelial Cell Vitality Measurements

Philipp Hinz[#], Mario Mueh, Jessica Heck, Christian Damm
Institute of Microwave Engineering, Ulm University, Germany
[#]philipp.hinz@uni-ulm.de

***Abstract* — A novel measurement setup for contact-free live monitoring of cell vitality using a G-band dielectric waveguide (DWG) from 140 GHz to 220 GHz is introduced. Static and time-variant error influences caused by temperature expansion and water evaporation are investigated, modeled, and compensated. The resulting measured scattering parameters allow the observation of small changes within the signal reflected by the cell suspension. Through using UV-C radiation, the cells can be influenced within the setup. Finally, an exemplary measurement on yeast cells is presented, which demonstrates the capability of the DWG for contact-free measurements.**

***Keywords* — Microwave sensors, biosensors, dielectric waveguide, millimeter wave, cells.**

I. Introduction

The vitality of epithelial cells is an important figure of merit for the human physiology. Especially the lung tissue is of utmost interest e.g. for drug research, as it contains cell monolayers, which are responsible for gas exchange during aspiration. These cells are crucial for the simultaneous supply of fresh oxygen and disposal of carbon dioxide.

Measuring the transepithelial electrical resistance (TEER) is the state-of-the-art method for measuring cell vitality. This is a contact-based setup where the cell is being covered with an electrolyte, and the impedance is measured by using two electrodes above and below the monolayer [1]. Within the lower kHz region, a correlation between the impedance and cell vitality can be found. Since this method disturbs the natural environment of epithelial cells with one side facing the blood vessels and the other side facing the air within the lungs, it directly influences the measurand.

Using electromagnetic waves for cell measurement has already been established and modeled starting from 1 Hz [2] to multiple GHz [3]. Higher frequency ranges like the G-band from 140 GHz to 220 GHz promise measurements in free space without the need of bringing cells in close proximity to microstrip lines. In this paper, a novel technique will be presented providing a non-interacting and contact-free measurement method for epithelial cells. The proof-of-concept is performed with widely common yeast cells, since these are far easier to handle and cheaply available in every supermarket.

II. Cell Cultures

In many medical laboratories, epithelial cells can be found as in vitro cell cultures growing on a polymer membrane in a controlled environment. Usually, an incubator provides the necessary atmosphere, while the cells are fed with a nutrition liquid through the membrane mostly made of polyethylene terephthalate (PET) below. Normally, the cells originate from human or animal tissue. They are therefore neither cheap nor handled in a microwave laboratory due to biosafety regulations.

To overcome these problems, the example measurements in this work are performed with yeast cells of the species *Saccharomyces cerevisiae*. Under ideal circumstances the generation time is around 80 min. This means that the cell count in a suspension doubles within that time. Single cells are 1 µm to 10 µm in size and have an ovoid shape as shown in Fig. 1b. They can appear as single cells or build up clusters. Yeast cells show already a noticeable metabolism at room temperature, which eliminates the need of an incubator. [4]

For the measurements, a nutrition liquid is mixed to keep the cells in a suspension. The liquid contains deionized water as a base with added salt (sodium chloride) and saccharose. Yeast cells are mixed in equal parts by mass with the liquid. Afterwards, the suspension is added onto a membrane within a well insert as shown in Fig. 1a.

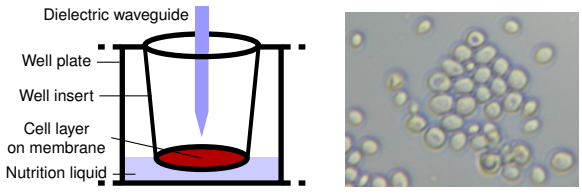

Fig. 1. (a) Schematic view of a cultivated well insert within a well plate with nutrition supply. (b) Yeast cells *Saccharomyces cerevisiae* under a light microscope in solution with low concentration.

III. Measurement Setup

A schematic overview of the measurement setup is shown in Fig. 2. For the acquisition of S-parameters, a Keysight N5247A vector network analyzer is used in combination with two VDI-WR5.1 140 GHz to 220 GHz frequency extension modules. The second unit is only required to perform a TRL calibration of the hollow waveguide. A mode converter is connected to the calibrated flange to feed the dielectric waveguide (DWG) in HE_{11}-mode [5]. The DWG is guided in around 2 mm distance orthogonal to the cell film surface

within the sample holder. The measurement stage is enclosed in a ventilated box to establish a controlled forced airflow, preventing the accumulation of heat introduced by the equipment. Two PT100 temperature probes are used for temperature logging within and outside of the box.

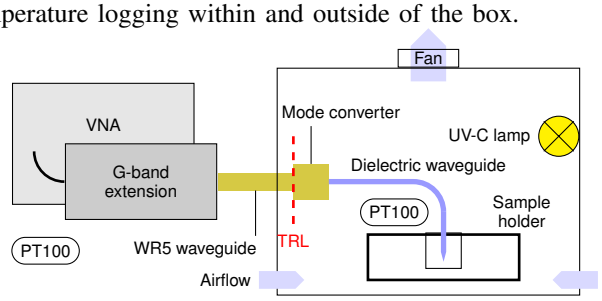

Fig. 2. Overview of the measurement setup. Parts of the setup are enclosed to shield the UV radiation. An attached fan ensures a constant airflow. The TRL calibration reference plane is marked with a dashed line (– – –).

A. Dielectric Waveguide

The dielectric waveguide is made of high-density polyethylene (HDPE) with ε_r=2.25, which is machined to a rectangular shape. It measures 1295 µm by 648 µm in profile and 20 cm in length. The frequency-dependent field distribution of the hybrid HE_{11}-mode causes dispersive propagation. At lower frequencies, a significant part of the field is guided outside of the waveguide and can interact with materials in close proximity. This effect is reduced with increasing frequency. From 140 to 220 GHz the transmission line losses amount to around 2.5 to 8 $\mathrm{dB/m}$ respectively. [5]

To couple the signal from the DWG into free space, the broad edge of the tip is tapered over 3 mm as depicted in Fig. 3. Due to the frequency-dependent field distribution, this leads to dispersive radiation characteristics as shown in Table 1. The results have been obtained with a full-wave simulator.

Table 1. Simulated radiation gain and rotation symmetric beam width of the dielectric waveguide tip at different frequencies.

Frequency	Gain	3 dB-angular width
140 GHz	16.2 dBi	27.1°
160 GHz	15.0 dBi	30.9°
220 GHz	14.0 dBi	39.6°

B. UV-C Treatment

To evaluate the correlation of the measured signal and the cell viability, the yeast cell metabolism should be disturbed without mechanical changes in the system. UV-C light is used since the exposure leads over long terms to severe cell damage and change of the surrounding medium [6], [7]. During one radiation interval, both 6 W low pressure mercury vapor lamps are turned on for 5 min. With the assumption of mostly all electrical energy converted to heat, 3.6 kJ of thermic energy is introduced into the box. This is enough to heat the box air volume of 80 L by around 36 K.

IV. Error Influences

Due to the complex measurement setup, multiple error influences are introduced. Most of them are static and less important to relative measurements. Time variant influences are critical, since they overlap the weak and slow response from the cell material.

A. Static Error Influences

The proposed measurement setup introduces invariant errors on the acquired S-parameters. Ideally, one would calibrate in front of the dielectric waveguide tip, but no standard calibration method is applicable to solve this problem. To minimize the influence of the static errors dominated by the mode converter, two reasonable normalization reference measurements are taken as shown in Figs. 3a and 3b. Similar to short-open-match calibration, a short is used to specify the reference plane, and a match to determine unwanted in-path reflections. The normalized S-parameters are calculated under consideration of the reflector phase as

$$S_{11,\mathrm{norm}} = \frac{S_{11,\mathrm{meas}} - S_{11,\mathrm{match}}}{S_{11,\mathrm{short}} - S_{11,\mathrm{match}}} \mathrm{e}^{-\mathrm{j}\pi}. \tag{1}$$

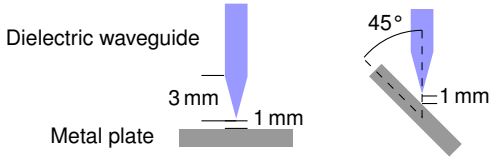

(a) Short. (b) Match.

Fig. 3. Schematic view of the normalization reference measurements.

For these reference measurements, the distance between the dielectric waveguide tip and the metal surface was chosen as 1 mm. The residual error after the normalization can be seen in an example measurement of a metal plate in 2 mm distance in Fig. 4. The error is dominated by a resonance from a standing wave with a free spectral range of approx. 0.5 GHz. This corresponds with ε_r=2.25 to a length of

$$l = \frac{c_0}{2f\sqrt{\varepsilon_r}} \approx 20\,\mathrm{cm} \tag{2}$$

and matches the length of the dielectric waveguide.

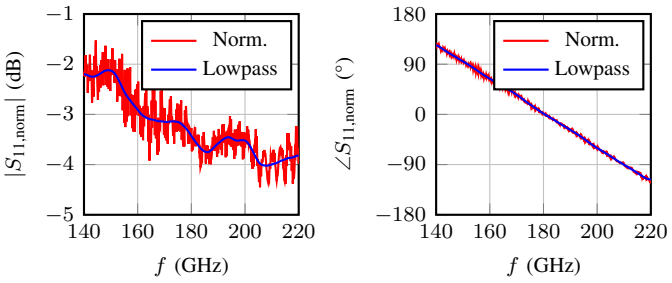

Fig. 4. Sample measurement of a metal surface in 2 mm distance. Reference measured in 1 mm distance. Red shows signal after normalization, blue with additional lowpass filtering.

The residual error, caused by reference-plane mismatch, is lowpass-filtered with a minimum-order infinite impulse response. Afterwards, the phase shows a predictable progression in Fig. 4. For the amplitude a linear trend is expected, since the beam width of the dielectric waveguide

tip is increasing with frequency. Unfortunately, this trend is superimposed with an error source, which is not yet known. Since the DWG has poor phase stability due to its flexibility, the reference measurements should be repeated whenever the waveguide is moved.

B. Temperature-Related Changes

Natural materials change their size in dependence of temperature. This property is described by the linear temperature expansion coefficient α_{exp} given for HDPE as $120\,\mu\text{m}/(\text{m}\cdot\text{K})$ [8]. This yields the temperature dependent change in length

$$\Delta l = l_0 \alpha_{\text{exp}} \Delta T. \tag{3}$$

Due to the expected change of $24\,\mu\text{m}/\text{K}$ over 20 cm, loss variation can be neglected but changes in the measured phase cannot. The phase constant β derives from the propagation constant

$$\gamma = \alpha + \text{j}\beta, \tag{4}$$

where β can be assumed with $\mu_{\text{r,eff}}$=1 as

$$\beta = \frac{\omega l \sqrt{\varepsilon_{\text{r,eff}}}}{c_0} \tag{5}$$

with the angular frequency ω and the effective permittivity $\varepsilon_{\text{r,eff}}$. However, the measured phase change is not fully explainable by this approach. Additional measurements where conducted to observe the phase variation over temperature of a reflection coefficient measurement of a metal reflector, while the temperature within the enclosure is slowly increased and recorded with 10 mK precision in 5 cm distance of the waveguide without ventilation. Using the acquired data, a temperature dependent β is determined as

$$\beta(\Delta T) = l \Delta T (m 2\pi f + b) \tag{6}$$

with fitted m=−2.918 13·10^{-4}, b=0.529 72, and f given in GHz. The resulting phase change is depicted in Fig. 5 compared to the expected change by temperature expansion. This shows an unforeseeable temperature dependency of $\varepsilon_{\text{r,eff}}$, since the phase change is decreasing with frequency and is only to some extent caused by the normalization in (1).

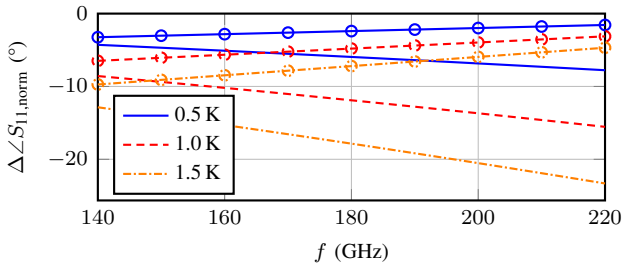

Fig. 5. Expected change of the phase progression for a reflection signal through a 20 cm long HDPE-DWG at $\Delta T = 0.5, 1, 1.5$ K. Curves without marks (——) show the temperature expansion model from (5), marks (—o—) show the actual model from (6).

The modeled temperature dependency is now validated in a measurement as in Fig. 3a, equivalent to the previous one. The temperature was increased with the help of an incandescent lamp by 2.5 K over 8 min. The raw influence on the phase referenced to the first measurement is shown in Fig. 6a. In Fig. 6b, the temperature compensation has been applied. The phase variation could be reduced from 18° to 3°. The remaining error can be explained by insufficient settling time and discrepancy to the DWG of the temperature sensor.

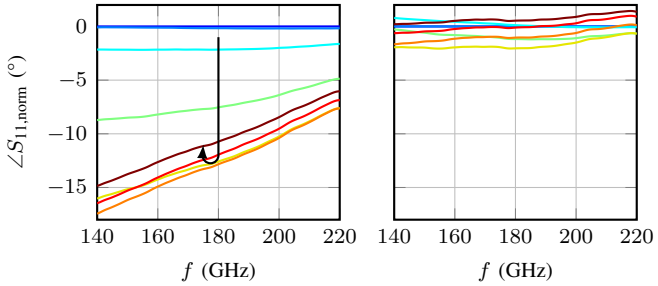

(a) No compensation. (b) Temperature compensated.

Fig. 6. Measured phase change of a metal reflector referenced to the first measurement at 0 min (——) in 1 min steps, until 7 min (——). The temperature was increased within 5 min (——) by 2.5 K without ventilation.

Another influence besides the temperature expansion of the waveguide is the permittivity of water, which is known to be highly temperature dependent [9]. Only a fraction of the heat energy from the UV-C lamps is absorbed by the cell suspension and nutrition liquid. Since the heat capacity of 1 L of water is 3500 times higher than that of an equal air volume, its temperature rise is neglected. Whereas the temperature dependency of the cell suspension is not known, it is important to stabilize the environment temperature of the setup.

C. Evaporation-Related Changes

Hence the measurements are not taken in an atmosphere with 100 % relative humidity, the evaporation of water in the sample must be considered. This results in two effects: The thickness of the sample reduces, and the solute concentration increases. Under ideal circumstances, the cell suspension and nutrition liquid have a constant salt concentration due to osmosis. The porous membrane of the well insert allows the concentration on both sides to be in equilibrium. Since osmosis is a rather slow process, the evaporation dominates.

The evaporation rate E is increased by the introduction of a fan within the setup. Hisatake et al. [10] stated that E is proportional to the square root of the air flow velocity v at the surface of a water reservoir, whereas the temperature difference of air and liquid is far more important than the ambient temperature. The influence on the measured phase can be assumed with an additional piece of line in free space as in (5) with $\varepsilon_{\text{r,eff}}$=1. The length l equals twice the height reduction of the sample mixture.

In addition to the introduced temperature compensation, the influence of evaporating water could be compensated under the assumption of E=0.065 with v=0.01 m/s, and 50 % relative humidity [10]. The according measurement of a well insert loaded with 6 µL soap water to overcome adhesion in 2 mm

distance is shown in Fig. 7. The reflection phase in Fig. 7a is referenced on the initial measurement. With a measurement interval of 5 min, a trend is noticeable correlating with an enlarging line delay. In Fig. 7b the presented temperature and evaporation compensation is applied, showing a minimized overall trend. The now increasing ripple is due to the reference plane shift, caused most likely by a standing wave with $\Delta f \approx 60\,\mathrm{GHz}$, matching with (2) for air the distance of 2.5 mm between the DWG tip and the sample surface. Better performance is achieved by more precise temperature measurement.

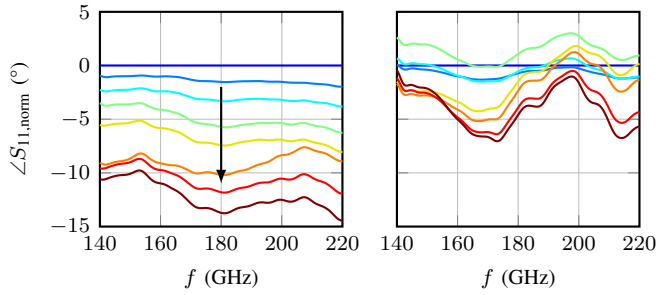

(a) No compensation.

(b) Temperature and evaporation compensated.

Fig. 7. Measured phase change of a well insert loaded with 6 µL soap water referenced to the first measurement at 0 min (——) in 5 min steps until 35 min (——). During measurement at 25 min (——), the UV lamps were turned on for 5 min. The setup was ventilated to minimize heat accumulation.

V. Example Measurement

Finally, an example measurement of yeast cells loaded onto a well insert is performed. 15 µL of cell suspension is added on the membrane and distributed equally. A larger volume is necessary, since the cell suspension has a higher surface tension than soap water and leads to a meniscus at the edge of the membrane. Prior to recording the results, the suspension is given 20 min settling time. The measured phase change shown in Fig. 8a against the first measurement without compensation might be mistaken for a significant change within the sample. However, once the presented temperature and evaporation compensation is added in Fig. 8b, the remaining changes in the phase are now dominated by actual changes of the suspension and the cells itself, which is influenced by the UV-C irradiation. A small change in the trend over time is observable and must be further investigated over a longer time period.

VI. Conclusion

A novel measurement setup for cell vitality monitoring using a dielectric waveguide at mm-wave frequencies has been introduced. Static errors within the reflection coefficient caused by the setup itself could be compensated with an acceptable residuum. The dominating dynamic errors were named and compensated based on a model of evaporation and temperature expansion. Nevertheless, it is important to stabilize the environmental conditions for a clearer identification of the actual cell response on the measurement signal. Short-time thermal changes introduced by the heat dissipation,

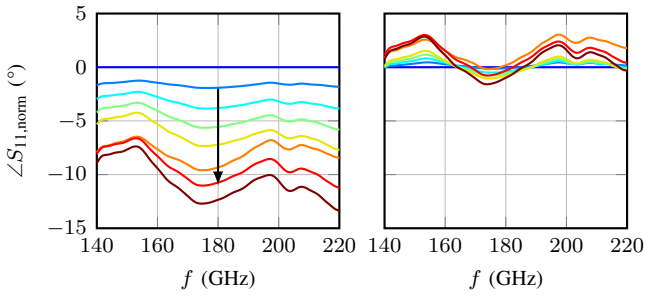

(a) No compensation.

(b) Temperature and evaporation compensated.

Fig. 8. Measured phase change of a well insert loaded with 15 µL cell suspension referenced to the first measurement at 0 min (——) in 5 min steps until 35 min (——). During measurement at 25 min (——) the UV lamps were turned on for 5 min. The setup was ventilated to minimize heat accumulation.

for example of UV-C lamps, can be compensated with precise knowledge of the temperature close to the dielectric waveguide. Further investigations on the suspected temperature dependency of HDPE-DWGs must be done.

Overall, the compensation of the different error influences allows the observation of very weak changes within the reflected signal.

Acknowledgment

We acknowledge the funding of this work within the research training group GRK 2203/1 (Mikro- und nanoskalige Sensorik für die Lunge). We also acknowledge the support of Prof. Dr. Manfred Frick from the Institute of General Physiology, Ulm University.

References

[1] K. Benson, S. Cramer, and H.-J. Galla, "Impedance-based cell monitoring: barrier properties and beyond," *Fluids and Barriers of the CNS*, vol. 10, no. 1, Jan. 2013.

[2] H. P. Schwan, "Electrical properties of tissues and cell suspensions: mechanisms and models," in *Proc. 16th IEEE Annu. Int. Conf. Eng. Med. Biol. Soc.* IEEE, 1994.

[3] K. Grenier, D. Dubuc, T. Chen, F. Artis, T. Chretiennot, M. Poupot, and J.-J. Fournie, "Recent advances in microwave-based dielectric spectroscopy at the cellular level for cancer investigations," *IEEE Trans. Microw. Theory Tech.*, vol. 61, no. 5, pp. 2023–2030, May 2013.

[4] H. Feldmann, Ed., *Yeast*. Wiley-VCH Verlag GmbH & Co. KGaA, Aug. 2012.

[5] M. Geiger, "Flexible Wellenleitermesssonde für MMIC-basierte Radarsysteme bis 300 GHz," Ph.D. dissertation, Universität Ulm, 2021.

[6] J. N. Davidson, "The effect of ultraviolet light on living yeast cells," *Biochemical Journal*, vol. 34, no. 12, pp. 1537–1539, Dec. 1940.

[7] F. W. Tanner and J. R. Byerley, "The effect of ultraviolet light on the fermenting ability of yeasts," *Archiv für Mikrobiologie*, vol. 5, no. 1, pp. 349–357, 1934.

[8] G. Abts, *Kunststoff-Wissen für Einsteiger*. München: Hanser, 2016.

[9] T. Meissner and F. Wentz, "The complex dielectric constant of pure and sea water from microwave satellite observations," *IEEE Trans. Geosci. Remote Sens.*, vol. 42, no. 9, pp. 1836–1849, Sep. 2004.

[10] K. Hisatake, S. Tanaka, and Y. Aizawa, "Evaporation rate of water in a vessel," *Journal of Applied Physics*, vol. 73, no. 11, pp. 7395–7401, Jun. 1993.